Charge transport in mesoscopic conducting polymer wires

2008 J. Phys.: Condens. Matter 20 374120

(http://iopscience.iop.org/0953-8984/20/37/374120)

IOP PUBLISHING JOURNAL OF PHYSICS: CONDENSED MATTER

J. Phys.: Condens. Matter **20** (2008) 374120 (8pp) doi:10.1088/0953-8984/20/37/374120

Charge transport in mesoscopic conducting polymer wires

Jin He[1,6], Erica S Forzani[2], Larry A Nagahara[3,7], Nongjian Tao[2] and Stuart Lindsay[1,4,5]

[1] Biodesign Institute, Arizona State University, Tempe, AZ 85287, USA
[2] Department of Electrical Engineering and the Center for Solid State Electronics Research, Arizona State University, Tempe, AZ 85287, USA
[3] Embedded Systems Research Center, Motorola Labs, Tempe, AZ 85284, USA
[4] Department of Chemistry and Biochemistry, Arizona State University, Tempe, AZ 85287, USA
[5] Department of Physics and Astronomy, Arizona State University, Tempe, AZ 85287, USA

E-mail: JinHe@asu.edu

Received 13 February 2008, in final form 3 March 2008
Published 26 August 2008
Online at stacks.iop.org/JPhysCM/20/374120

Abstract

In an attempt to reconcile transport in aniline oligomers with that observed in bulk polyaniline, we constructed meso-scale (60 nm) molecular junctions bridged by polyanion-stabilized polyaniline (PANI) strands. Junctions were characterized by their conductance versus electrochemical potential (G–E) and current versus voltage (I–V) characteristics, In contrast to bulk polyaniline, sharp peaks were seen in the G–E data, and these gave rise to negative differential resistance in the I–V curves, behavior much like that observed in aniline oligomers. The width of the conductance peaks increased with the amount of polymer deposited in the junction. In contrast to oligomers, the peaks in the meso-scale devices displayed a large hysteresis. The absolute conductance of the junctions is far too high to be consistent with transport along isolated chains, suggesting that a fundamental charge carrying unit is something morphologically more complex than a single polymer molecule.

1. Introduction

Our usual picture of a 'conductor' is based on metals in which quasi-particles excited near a Fermi surface behave like a free electron gas. The situation is fundamentally different in one dimension where no Fermi surface can exist. Fermi liquid theory is replaced by Luttinger theory with very different excitations [1]. One-dimensional systems cannot, in principle, transport 'free' electrons because all charge displacements must be highly correlated. The discovery of conducting polymers [2] is all the more remarkable in this regard. Polyaniline is among the most studied of conducting polymers. Its conductivity depends strongly on its oxidation state. Wrighton *et al* [3] built micron-scale electrochemical transistors consisting of polyaniline fiber bundles grown electrochemically across an electrode gap and immersed in a supporting electrolyte. Measurements of the conductance (G) versus electrochemical potential (E) of the junctions at a fixed bias showed a smooth, broad transition between insulating and conducting states, with current–voltage (I–V) characteristics that were linear. The bulk oxidized material is in fact capable of true metallic behavior if crystalline enough, as demonstrated by a reflectance characteristic of free carriers [4].

In contrast, a recent study of aniline oligomers under potential control [5] showed that the G–E curves pass through a sharp maximum near the formal potential for the first oxidation, a common occurrence for tunnel transport in redox-active molecules [6]. This work by Chen *et al* showed predominantly averaged data, but some single molecule data were presented. The conductivity maximum gave rise to negative differential resistance in the I–V curves because the local potential was strongly affected by the bias applied across the junction [5]. Thus, as increasing applied bias changed the oxidation state of the molecule, the conductance fell dramatically. Furthermore, the peak conductance (of about 6 nS for a heptamer) was several orders of magnitude smaller than the conductance expected in a single 'metallic'

[6] Author to whom any correspondence should be addressed.
[7] Present address: National Institutes of Health, Bethesda, MD 20892, USA.

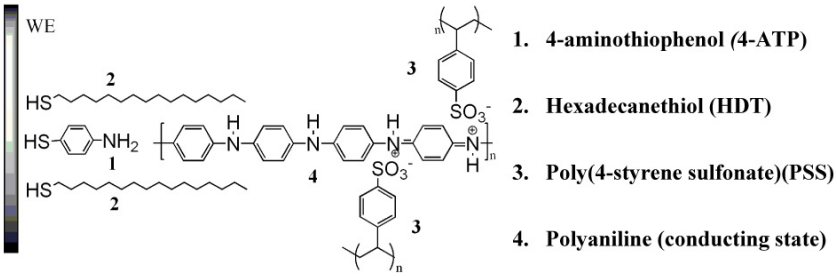

Scheme 1. Polyanion-stabilized polyaniline structures.

channel (i.e. 77 μS). A study of trimers, pentamers, and heptamers [7] showed a remarkably small inverse decay length ($\beta \sim 0.4$ per added monomer for the neutral molecule and 0.3 for the oxidized molecule). These small inverse decay lengths do not agree with first-principles calculations of tunnel transport [8], suggesting that some other mechanism operates in these oligomers. Small though these inverse decay lengths are, we shall show that they are completely incompatible with the notion of single-chain transport in mesoscopic devices.

In an attempt to reconcile the very different behavior of bulk polyaniline and polyaniline oligomers, we have constructed mesoscopic devices consisting of a small number of molecules bridging a 60 nm electrode gap. The behavior of polyaniline in small gaps has been previously studied [9, 10] but with little control over the number of molecules bridging the gap. Here, we characterize the amount of polymer in the gap electrochemically and have observed systematic differences in behavior with the amount of material grown in the gap. With a small number of polyaniline chains bridging the gap, sharp conductance peaks are seen in the G–E curves with corresponding sharp NDR peaks in I–V curves. This is similar to the behavior recorded from single aniline oligomers. With increasing amount of polyaniline bridging the gap, much broader peaks appear in G–E curves and the I–V curves become linear, consistent with other polyaniline junction devices reported to date. The behavior observed in the mesoscopic devices studied here does show aspects of both bulk and oligomer properties, although aspects of the behavior have no simple explanation in either tunneling or 3D hopping theory, pointing to a need for a new theoretical framework for understanding transport on the meso-scale in these quasi-one-dimensional systems.

2. Experimental methods

2.1. Aniline device preparation

Two 25–30 nm thick gold nanoelectrodes with 60 ± 20 nm spacing were fabricated on an oxidized silicon substrate using optical and electron beam lithography (figures 1(a) and (b)). The radius of the electrodes in the junction was approximately 20 nm. The nanoelectrode arrays were covered with a Si_3N_4 insulation layer (except for a small window directly over the gaps) to reduce leakage current due to ionic conduction through the electrolyte. Before use, the chips were immersed in acetone for 5 min and cleaned by UV ozone to remove a protective poly(methyl methacrylate) (PMMA) layer. The chips were further rinsed with ethanol for 5 min, dried with nitrogen and immediately immersed in an ethanol solution containing 1–9 mM of 4-aminothiophenol **1** (scheme 1) (Aldrich, 97%) or a mixture of **1** and hexadecanethiol **2** (scheme 1) (Aldrich, 97%) in either 1:1 or 1:3 molar ratios [11, 12] to produce either aminophenol functionalized electrodes or electrodes in which the aminophenol was diluted in an alkane matrix.

2.2. Polyaniline deposition

After incubation overnight with the thiols, the device was copiously rinsed with ethanol followed by a brief rinse with deionized (DI) (18 MΩ cm) water. It was transferred to a probe station and covered with a polydimethylsiloxane (PDMS) liquid cell. A homemade bipotentiostat was used to control the potentials of the two electrodes, each one of which functioned as a working electrode. Silver and platinum wires were cleaned by sonication in acetone, ethano, and DI water and the platinum wire used as a counter electrode (CE, figure 1(c)) and the silver wire used as quasi-reference electrodes (RE, figure 1(c)). The platinum wire was further cleaned in a hydrogen flame. The silver wire quasi-reference electrodes were calibrated against $Ag/AgCl/Cl^-$ (3 M) reference electrode ($E_{AgCl} = 0.0$ V) in a 50 mM H_2SO_4 solution showing a difference of 0.10 V ($E_{Ag} + 0.1\ V = E_{AgCl}$). All potentials are referred to the Ag wire quasi-reference electrode in this paper. Polyaniline was deposited onto the electrodes by sweeping the electrochemical potential between −0.1 and 0.6 V (versus Ag wire) in 0.12 M aniline + 0.5 M H_2SO_4 + 0.13 M $NaHSO_4$ + 2.67 mg ml^{-1} poly(4-styrene sulfonate) (**3** in scheme 1) (7000 g mol^{-1}) at 50–70 mV s^{-1} [13]. The bias applied between two working electrodes was 10–50 mV. The growing PANI strands started to bridge the gap after about 7 min, as indicated by a sharp current increase. The potential cycle was repeated up to six times, with the amount of aniline polymerized being characterized by integrating the charge under each deposition peak. The first oxidation peak position corresponding to the redox transition from leucoemeraldine to emeraldine was stable at 40 ± 11 mV in the supporting electrolyte used for electropolymerization at pH = 0. The position shifts positively by about 50 mV in pH = 1 (50 mM H_2SO_4) solution. The device was gently rinsed with DI water and measured in a bare support electrolyte (50 mM H_2SO_4).

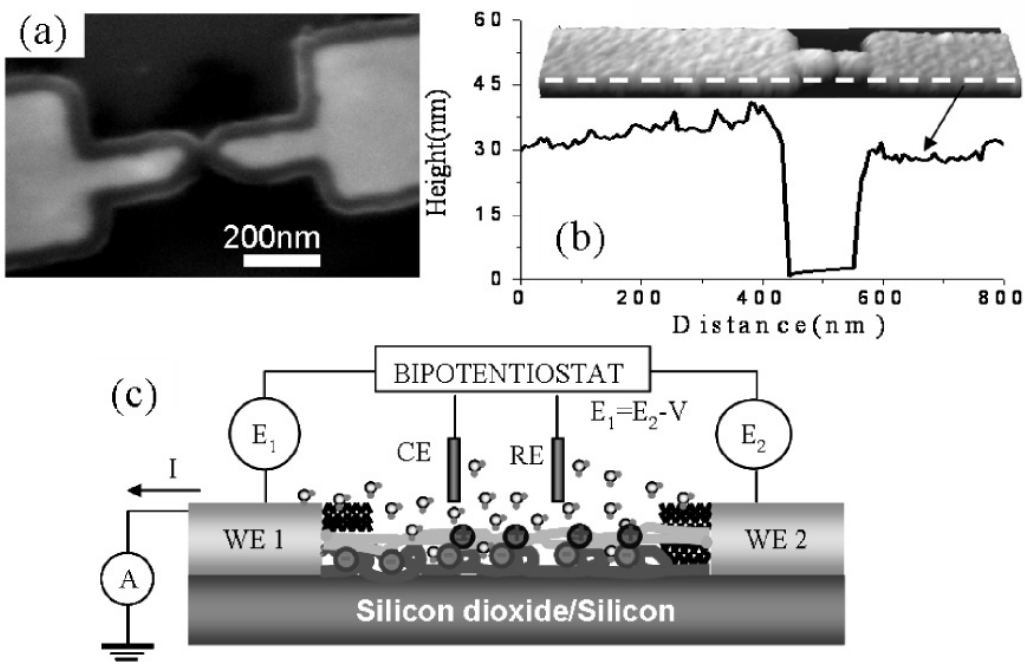

Figure 1. (a) SEM image of a typical junction containing PANI (evident as a thin film around the edges of the electrode). (b) AFM scan (inset) of a junction together with a height trace across the gap. (c) Schematic layout of the electrochemical control and measurement system for the junctions.

2.3. Electrical measurement

PANI nanojunctions were connected via a probe station located inside a Faraday cage and the current was measured by a Keithley low noise current picoammeter. The electrical measurement setup is shown schematically in figure 1(c). The potential at WE 1 was defined as E_1 and the potential at WE 2 was defined as E_2. The bias V is defined as E_2–E_1. For G–E measurements, a fixed small bias (typical −10 mV) was applied between two electrodes (WE 1 and WE 2) while the potential, E_2, was swept (E_1 was also swept to keep the bias across the junction fixed). For I–V measurements, E_2 was fixed with respect to the reference electrode and E_1 was swept. All the signals were displayed and collected by a digital oscilloscope (Yokogawa DL 708).

3. Results and discussion

The formation of stable small junctions required the use of an anionic interlayer (poly(4-styrene sulfonate)—PSS) [14, 15] while a uniform growth pattern was established using the aminothiophenol groups as anchors to the electrodes. More uniform growth was achieved with monolayers diluted with the alkanethiol [15, 11]. Energy dispersive spectrometry (EDS) spectroscopy (see appendix A) showed that PSS uniformly covered the silicon dioxide surface before the polymerization of PANI. Figure 1(b) shows an atomic force microscopy (AFM) image of a PANI/PSS nanojunction with a height profile displayed below. The average thickness of polymer layer is around 2–3 nm, given the initial gold height of 25–30 nm. The AFM profile shows preferred growth from electrode edges. In this case, WE 1 was more positive than WE 2 so that the polymerization started from WE 1. An scanning electron microscope (SEM) image (figure 1(a)) shows uniform polymer coating on electrodes, in dramatic contrast to the amorphous structure of PANI formed in the absence of aminothiophenol (ATP) and PSS (figure A.1).

Cyclic voltammograms (CVs) taken during the electropolymerization of aniline (figure 2) show the first oxidation potential of polyaniline near 0 V with the second beyond 0.6 V. The thickness of the polyaniline layer was estimated to be smaller than 4 nm based on the anodic Faradaic current of the first oxidation peak in the last CV recorded before PANI bridging (shaded area, figure 2(a)), supporting the AFM estimate of the film thickness. *In situ* CVs collected at pH = 0 right before (dashed curve) and after polymer bridging (solid curve) are shown in figure 2(b). A current peak appeared above the Faradaic and charging current background as the first sign of polymer bridging. Continued deposition of polyaniline resulted in the transport signal (gray shading in figure 2(b)) completely swamping the background electrochemical current, and this total current was used as a relative measure of the amount of polyaniline in the junction.

Junctions terminated immediately after bridging yielded G–E curves with sharp conductance peaks as shown in figure 3(a). The width and magnitude of the current peak in G–E curves are found to increase with the number of deposition potential cycles counted after the first appearance of a current jump (figure 2(b)). We used this phenomenon to control the number of PANI strands bridging the junction. An example of a G–E curve obtained immediately after bridging is shown

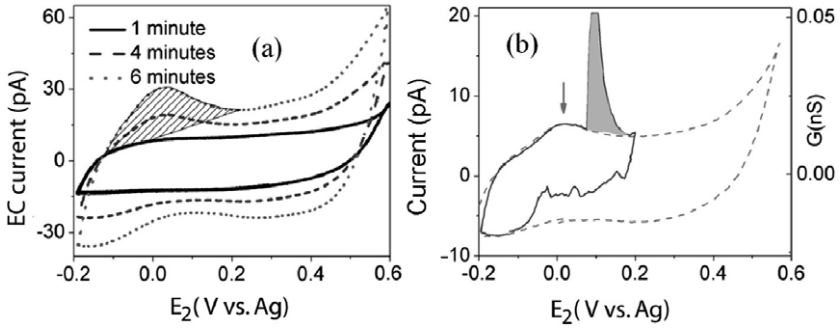

Figure 2. (a) Cyclic voltammograms (CVs) collected prior to bridging the nanogap. The shaded region shows the part of the sweep integrated over all sweeps to estimate the amount of deposited PANI. (b) Sweep just before (dashed line) and just at bridging (solid line). The amount of PANI deposited in junctions terminated at this point could be calculated directly. The direct conductance (shaded region) grows to swamp the electrochemical signal on further cycling so the total charge is used as a relative measure of the amount of PANI. The arrow shows the oxidation peak still visible at this point.

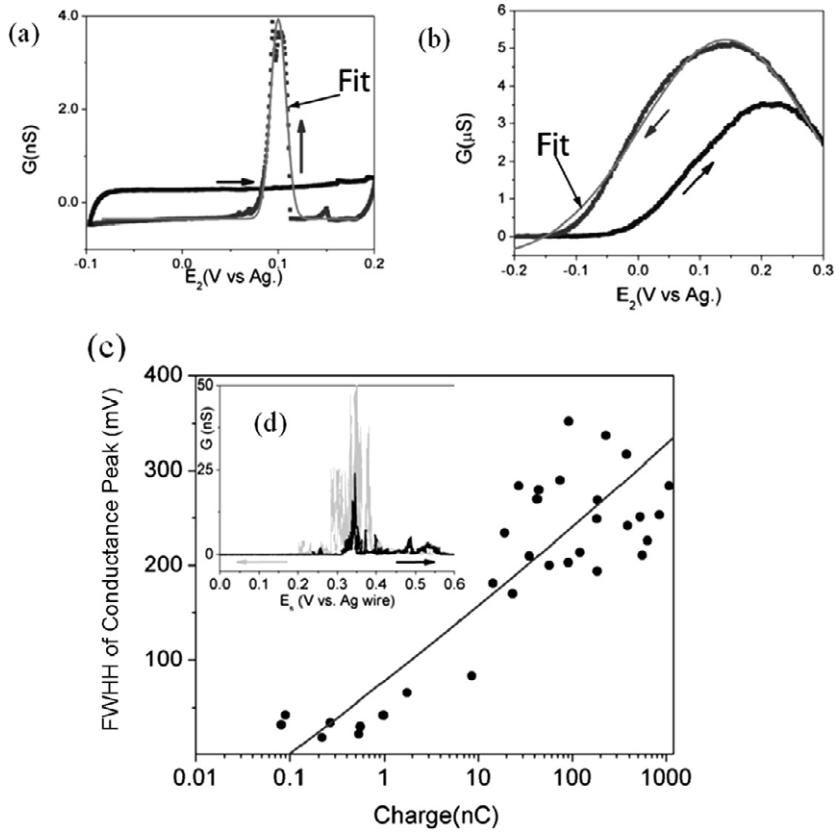

Figure 3. *G–E* curves for (a) a junction with little PANI and (b) a junction with a larger amount of PANI. Lines are fits to equation (1). Arrows show the cycling direction. (c) Scatter plot of the width of *G–E* peaks versus the log of the integrated charge under the conductance peak in *G–E* curves. Junctions with more PANI have a wider conductance peak in *G–E* curves. (d) Representative *G–E* curve for a single molecule obtained with a scanning tunneling microscope. The dark line is the forward sweep and the gray line is the backward sweep.

in figure 3(a). The response is hysteretic. No peak appears on sweeping in the up (oxidizing) direction but a sharp peak appears on sweeping in the downward direction. An example of a *G–E* curve for a junction containing substantially more PANI is shown in figure 3(b). The curves in this more densely-filled junction resemble those reported earlier for micron-scale transistors [16, 17] and nm-scale PANI junctions [9, 10]. The conductance hysteresis is still present but a peak is now visible in both scan directions. We fitted the *G–E* peaks with a Gaussian (equation (1) below) parameterizing the curves by the full width at half height (FWHH). We characterized the amount of PANI in the gap using the total charge (integrating the area under the conductance peaks in *G–E* curves such as figures 3(a) and (b)) conducted by the junctions after bridging. Prior to the closing of the gap, an exact estimate of the amount of PANI in the gap is available by integrating the charge in each cycle under the deposition peak (figure 2(a)). These are the data that yield the

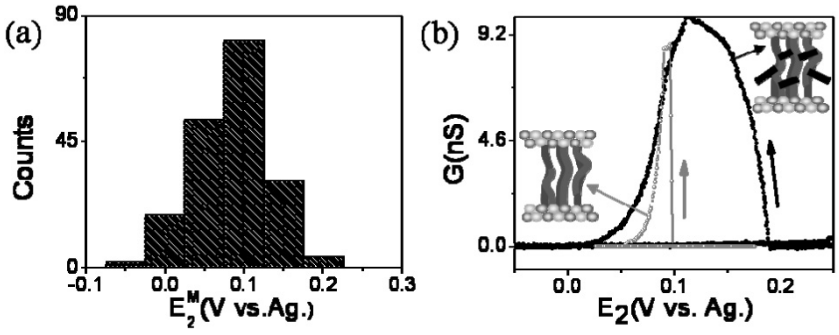

Figure 4. (a) Histogram of the potential at which the conductance peaks in the G–E curves. (b) G–E curve for a particular device before (darker trace) and after (lighter trace) chemical cross-linking of the PANI strands.

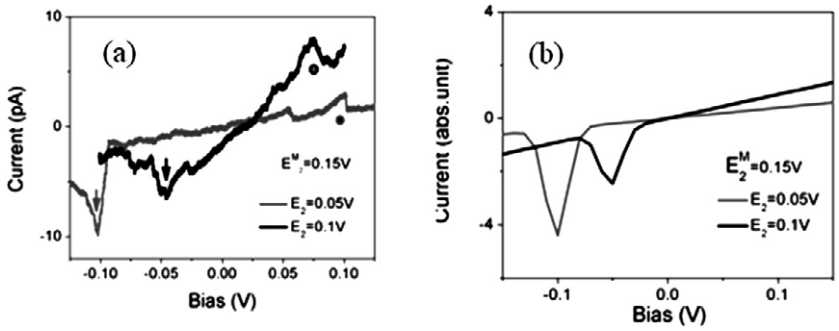

Figure 5. Negative differential resistance in a junction device. (a) I–V curves taken from a device with a sharp G–E curve at two values of surface potential. (b) I–V curves calculated for the device shown in (a) using equation (2).

estimate of the film thickness given earlier. After bridging, the current data rapidly become dominated by the conduction peak (figure 2(b)). This swamps the true electrochemical signal, but we take the integrated charge as a relative measure of the amount of material deposited based on the fact that the junctions with more deposited PANI have higher conductance. The FWHH of the conductance peak for a large number of junctions are plotted in figure 3(c) versus the logarithm of the integrated charge under the conductance peak. There is substantial scatter, not least because there are significant junction-to-junction variations (cf, figures 2(a) and (b)) but the width of the G–E peak clearly increases with the amount of PANI in the junction.

An example of a single molecule G–E curve, obtained for a heptamer in 50 mM H_2SO_4 [5] is shown in figure 3(d). Curves like these are difficult to obtain, highly variable, and noisy, but several features are common: (1) the peaks are generally very narrow; (2) the peaks are distributed around 0.3 V versus Ag, a little above the formal potential for the redox process [5]; (3) curves are often somewhat reversible, in sharp contrast to the extreme hysteresis that is always observed for the smallest meso-scale junctions (cf, figure 3(a)).

The G–E peaks in the mesoscopic device differ from the single molecule response in several respects. First, as mentioned above, the hysteresis is much more pronounced in the device. Second, the potential for maximum conductance is significantly lower (0.1 V—figure 4(a)) than that observed in single molecules (0.3 V [5]). Thirdly, the widths of the G–E peaks in the smallest devices are still substantially larger than (cf figure 3(a)) that observed in single molecules (cf figure 3(d)). We speculate that in even the smallest devices, interchain interactions are broadening the response compared to single molecule measurements. To test for this possibility, PANI strands were cross-linked through chemical reduction of the emeraldine salt by side groups of benzenedimethanethiol (see appendix B) [18]. Figure 4(b) shows G–E curves for the same device before and after modification. The width of the conductance peak increased substantially as a result of the increased interchain interactions.

A key goal of this work was to understand why negative differential resistance (NDR) is reliably observed in single molecules [5], but not in the devices studied to date [9, 10]. In fact, the less heavily loaded devices with sharp G–E peaks do indeed yield consistent NDR peaks in their response, and an example is given in figure 5(a). The NDR appears as the sharp dip labeled by an arrow (a second, unexpected feature is labeled with a dot). In order to demonstrate the essentially electrochemical nature of the NDR, we obtained I–V curves with the electrode WE 2 held at two different potentials. The peak NDR shifts linearly with E_2. If the sharp peaks do indeed correspond to a polaron band [19] (i.e. mediated by redox states) the potential dependence of the G–E curve can be fitted by a Gaussian function (Gerischer formula) as was done for an aniline oligomer [7].

$$G = G_0 + G_{\mathrm{M}} \exp\left(-2\frac{(E_2 - E_2^M - \alpha V)^2}{w^2}\right). \qquad (1)$$

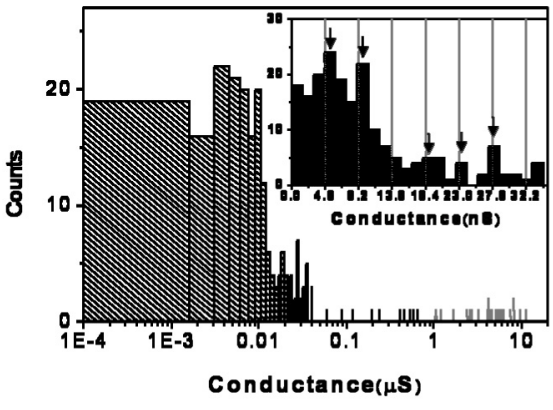

Figure 6. Histogram of the maximum conductance measured for all devices made. The inset is an expanded region showing some evidence of conductance quantization (arrows).

In equation (1), E_2^M is the potential of WE 2 where the device has maximum conductance, αV is the local potential change induced by the bias, V, applied across the device, with α a parameter that reflects the potential distribution in the gap [20]. G_0 is a background conductance, G_M the magnitude of the change on oxidation or reduction, and w parameterizes the (FWHH) of the Gaussian peak ($\sqrt{\ln 4}$ FWHH).

The I–V characteristics follow directly from equation (1) [5, 20]:

$$I(E_2, V) = GV = G_0(E_2)V + G_M \exp\left(-2\frac{(E_2 - E_2^M - \alpha V)^2}{w^2}\right) V. \quad (2)$$

Current–voltage (I–V) measurements were performed right after the G–E measurement (examples of which are fitted to equation (1) in figures 3(a) and (b)). The shape of the I–V curves changed dramatically with the amount of polyaniline in the junction changed. The junctions with large amounts of PANI in the junction yielded essentially linear curves with a small fall off in conductance at the highest bias, as reported by others [9, 10]. However, junctions with small amounts of PANI (and sharp G–E curves) yielded NDR peaks. We fitted the G–E profile for the junction used to obtain the I–V data shown in figure 5(a) with equation (1) and then used equation (2) to predict the corresponding I–V curves at two different potentials of WE 2. These are shown in figure 5(b). The agreement is excellent, although the theory presented here does not account for the additional features seen at large positive bias.

We determined the conductivity of the junctions in the conducting state from the peak of the G–E curves. These conductances varied over a wide range (figure 6) but it is clear that the majority of junctions lie in the 0.1–10 nS range. Are these values compatible with transport through individual polymer chains? Assuming a chain diameter of 0.5 nm and a maximum junction cross-section of 100 nm by 4 nm, the densest possible packing would result in 800 molecules spanning the gap. If the currents through each chain were additive, this would imply a conductance per polymer of about 0.1–10 pS. The peak conductance of a heptamer is 6 nS [5] and the smallest measured inverse decay length for the oxidized molecule is $\beta_N = 0.3$ per monomer of 0.57 nm length. Thus a polymer that spanned 60 nm would have a conductance of about 6 nS $\times$ exp[$-(105 \times 0.3)$] or 10^{-22} S, orders of magnitude smaller than the 0.1–10 pS estimated from the device conductance.

4. Conclusions

While PANI in small junctions show the emergence of features reminiscent of the properties of oligomers (sharp G–E curves, NDR in the I–V curves) the conduction process appears to be quite different. It is evidently not the 'tunneling-like' process observed in oligomers (though the small value of β in oligomers is not consistent with true tunneling either [7]) because this cannot account for the observed conductances. The larger hysteresis and shifted oxidation potential observed in the mesoscopic junctions suggest that a fundamentally different structural unit is involved in charge transport. Closer examination of figure 6 (inset) suggests that there may indeed be some quantization of the conductance distribution (arrows in the inset), the conductances being multiples of 4.6 nS. One possibility is that there is a critical smallest size of polymer bundle required for long-range charge transport. Such bundling would account for the hysteresis, because polymer–polymer contacts would exclude the ion diffusion required for redox processes. Thus a large overpotential would be required to drive the oxidation process, so that the redox-mediated current would only be observed following a previous oxidative cycling. Such a bundle would also explain the observation of a minimum width in the G–E curves that is always larger than that observed in single molecules.

Thus, in addition to the transition to true metallic behavior observed in highly ordered macroscopic PANI [4], it appears that there is a second type of structural rearrangement required on the meso-scale to bring about a bundle size that circumvents the geometrical constraints preventing free carrier propagation in truly one-dimensional systems [4].

Acknowledgments

This work was supported by the National Science Foundation through NIRT (ECS01101175). We gratefully acknowledge the use of SEM and EDS within the Center for Solid State Science (CSSS) at Arizona State University.

Appendix A. SEM image of the control device and energy dispersive spectroscopy (EDS) spectra

The SEM image shown in figure A.1 was taken on an aniline device that was prepared without utilizing ATP and PSS. Fiber shaped PANI and rough morphology were clearly observed.

EDS spectra were taken at an accelerating voltage of 20 keV and e-beam spot size 5 by EDAX EDS equipped at FEI XL 30 ESEM. Devices after each stage of the nanojunction

Table A.1. Sulfur and nitrogen element analysis results of aniline devices.

Device state	Device 1: after overnight immersion in ATP		Device 2: overnight immersion in ATP/HDT and 30 min immersion in PSS/aniline		Device 3: after PANI polymerization	
Element	Sulfur	Nitrogen	Sulfur	Nitrogen	Sulfur	Nitrogen
SiO_2 substrate near gold electrodes	No	No	Yes	No	Yes	Yes
Gold electrode	Yes	Yes	Yes	Yes	Yes	Yes

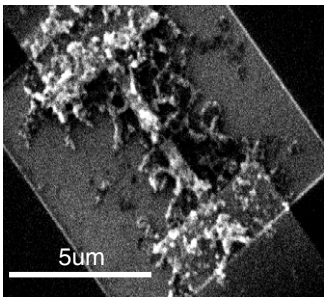

Figure A.1. SEM image of a PANI junction without any surface modification. The darker area was covered with silicon nitrogen layer for insulation. The gray region is the exposed SiO_2 surface. The gold electrodes were fully covered with PANI.

modification were used for collecting EDS spectra. The results are shown in table A.1. The sulfur element only exists in ATP, HDT, and PSS and nitrogen only exists in ATP and aniline. The presence of sulfur element and non-presence of nitrogen element on the silicon oxide surface near the gold electrode in device 2 demonstrated that the PSS layer covered the SiO_2 surface before the polymerization of aniline, acting as a preconcentrating layer of electrostatically adsorbed protonated aniline molecules during the electropolymerization process. A compact and layered structure, like PSS/PANI/PSS obtained by the ionic self-assembly process, was expected in the device and most probably helped the two-dimensional polyaniline growth along the SiO_2 surface between two gold electrodes.

Appendix B. Chemical modification of aniline

The polyaniline was kept at a potential of 500 mV (versus Ag/AgCl) for 5 min and immersed in 0.1 M benzenedimethanethiol (BDMT) solution for 30 min. The suggested structure of leucoemeraldine after modification is shown in figure A.2(a) [18]. The CVs before and after the modification are shown in figure A.2(b) (note that one of the CVs is shifted for the sake of clarity). The modification was also confirmed by Fourier transform-infrared (FTIR) spectra.

References

[1] Giamarchi T 2004 Theoretical framework for quasi-one dimensional systems *Chem. Rev.* **104** 5037–55
[2] Chiang C K, Fincher C R, Park Y W, Heeger A J, Shirakawa H, Louis E J, Gau S C and Macdiarmid A G 1977 Electrical-conductivity in doped polyacetylene *Phys. Rev. Lett.* **39** 1098–101
[3] Paul E W, Ricco A J and Wrighton M S 1985 Resistance of polyaniline films as a function of electrochemical potential and the fabrication of polyaniline-based microelectronic devices *J. Phys. Chem.* **89** 1441–7
[4] Lee K, Cho S, Park S H, Heeger A J, Lee C-W and Lee S-H 2006 Metallic transport in polyaniline *Nature* **441** 65–8
[5] Chen F, He J, Nuckolls C, Roberts T, Klare J and Lindsay S M 2005 A molecular switch based on potential-induced changes of oxidation state *Nano Lett.* **5** 503–6
[6] Lindsay S M 2006 Molecular wires and devices: advances and issues *Faraday Discuss.* **131** 403–9

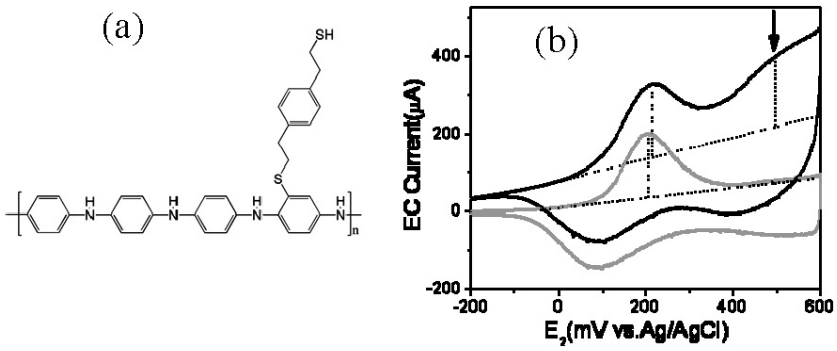

Figure A.2. (a) The suggested structure of BDMT cross-linking modified aniline at a reduced state. (b) The voltammograms before (gray) and after (black) the modification. The arrow near 500 mV indicates the redox peak due to the BDMT-modified PANI.

[7] He J, Chen F, Nuckolls C and Lindsay S 2007 Length dependence of charge transport in oligoanilines *Appl. Phys. Lett.* **90** 072112
[8] Lee M H, Speyer G and Sankey O F 2007 Theory of electron transport through single molecules of polyaniline *J. Phys.: Condens. Matter* **19** 215204
[9] Jones E T T, Chyan O M and Wrighton M S 1987 Preparation and characterization of molecule-based transistors with a 50 Nm source–drain separation with use of shadow deposition techniques—toward faster, more sensitive molecule-based devices *J. Am. Chem. Soc.* **109** 5526–8
[10] He H X, Zhu J S, Tao N J, Nagahara L A, Amlani I and Tsui R 2001 A conducting polymer nanojunction switch *J. Am. Chem. Soc.* **123** 7730–1
[11] Sabatani E, Gafni Y and Rubinstein I 1995 Morphology control in electrochemically grown conducting polymer-films. 3. A comparative-study of polyaniline films on bare gold and on gold pretreated with p-aminothiophenol *J. Phys. Chem.* **99** 12305–11
[12] Han D H and Park S M 2004 Electrochemistry of conductive polymers. 32. Nanoscopic examination of conductivities of polyaniline films *J. Phys. Chem.* B **108** 13921–7
[13] Genies E M and Tsintavis C 1985 Redox mechanism and electrochemical-behavior of polyaniline deposits *J. Electroanal. Chem.* **195** 109–28
[14] Wang J, Chan S, Carlson R R, Luo Y, Ge G, Ries R S, Heath J R and Tseng H-R 2004 Electrochemically fabricated polyaniline nanoframework electrode junctions that function as resistive sensors *Nano Lett.* **4** 1693–7
[15] Abaci S and Shannon C 2005 The influence of decanethiol/4-aminothiophenol mixed monolayers on the electrodeposition of polyaniline thin films *Electrochim. Acta* **50** 2967–73
[16] White H S, Kittlesen G P and Wrighton M S 1984 Chemical derivatization of an array of 3 gold microelectrodes with polypyrrole—fabrication of a molecule-based transistor *J. Am. Chem. Soc.* **106** 5375–7
[17] Kittlesen G P, White H S and Wrighton M S 1984 Chemical derivatization of microelectrode arrays by oxidation of pyrrole and N-methylpyrrole—fabrication of molecule-based electronic devices *J. Am. Chem. Soc.* **106** 7389–96
[18] Han C C, Hseih W D, Yeh J Y and Hong S P 1999 Combination of electrochemistry with concurrent reduction and substitution chemistry to provide a facile and versatile tool for preparing highly functionalized polyanilines *Chem. Mater.* **11** 480–6
[19] Yeganeh S, Galperin M and Ratner M A 2007 Switching in molecular transport junctions: polarization response *J. Am. Chem. Soc.* **129** 13313–20
[20] He J, Fu Q, Lindsay S M, Ciszek J W and Tour J M 2006 The electrochemical origin of voltage-controlled molecular conductance switching *J. Am. Chem. Soc.* **128** 14828–35